Article:
Ni, Z, Chu, F, Feng, Y et al. (2 more authors) (2021) Large-Scale Dewetting via Surfactant-Laden Droplet Impact. Langmuir, 37 (46). pp. 13729-13736. ISSN 0743-7463

https://doi.org/10.1021/acs.langmuir.1c02456

Large scale Dewetting via surfactant-laden droplet impact

Fuqiang Chu[1#], Zhongyuan Ni[2#], Yanhui Feng[1,*], and Dongsheng Wen[2,*]

[1]*School of Energy and Environmental Engineering, University of Science and Technology Beijing, Beijing 100083, China*

[2]*School of Aeronautic Science and Engineering, Beihang University, Beijing 100191, China*

[3]*School of Chemical and Process Engineering, University of Leeds, Leeds LS2 9JT, United Kingdom*

#F. Chu and Z. Ni contributed equally to this work.

**Corresponding authors; E-mails: yhfeng@me.ustb.edu.cn, d.wen@buaa.edu.cn*

Abstract

Dewetting phenomenon of a liquid film in the presence of surfactant exists in various natural, industrial, and biomedical processes, but still remains mysterious in some specific scenarios such as pulmonary surfactant therapy. Here, we investigate the dewetting behavior of water films initiated by surfactant-laden droplet impacting and show that the maximum dewetting diameter can even reach more than 50 times of the droplet size. We identify the S-type variation of the dewetting area and demonstrate its correlation to the dynamic surface tension reduction. From a viewpoint of energy conversion, we attribute the dewetting to the released surface energy caused by the surfactant addition, and establish a linear relation between the maximum dewetting and the surfactant concentration in the film, *i.e.*, $d_{max}^2 \propto c_{film}$, which agrees well with the experiments. These results may advance the physics of liquid film dewetting triggered by surfactant injection, which shall further guide practical applications.

Main Text

The Corona virus SARS-CoV-2 has affected more than 100 million confirmed patients since 2019 and this COVID-19 pandemic is still unstoppable [1]. SARS-CoV-2 may specifically destroy the type II alveolar cells [2-5], which produce protective lung surfactants to reduce the alveoli surface tension, thereby maintaining basic morphology and function of the alveoli and facilitating breathing [6-8]. In addition to the development of vaccine and treatment for COVID-19, various aspects about disease transmission and therapy have been studied including revealing the spreading mechanism of respiratory fluid droplets [9-11], fabricating robust self-cleaning objects or surfaces to repel virus [12,13], and improving some physical treatments such as UV irradiation [14,15] and surfactant therapy [16,17]. Here, we devote efforts to address some physical issues behind the pulmonary surfactant therapy which has been considered to have biological feasibility to alleviate or even cure COVID-19 associated acute respiratory distress syndrome [18-20].

Surfactant therapy is the medical administration of exogenous surfactant [21,22]. Surfactants are typically instilled directly into the trachea or aerosolized to be inhaled. In neonates with respiratory distress syndrome, surfactant therapy has proven to be efficacious, but unfortunately, in adults with acute respiratory distress syndrome it fails to demonstrate obvious beneficial effect [23,24]. From the clinician's perspective, several factors may influence the surfactant response, such as composition or dose of surfactant, technique of instillation, and timing of administration [25]. While from the view of physics, we infer that the stability of the liquid film after surfactant input is one of the key factors that determines the clinical efficacy of the surfactant therapy. As a kind of typical instability behavior, the possible dewetting phenomenon in pulmonary liquid film after surfactant instillation may have adverse effects by destroying the integrity and uniformity of the liquid film, which means, it is better to avoid the dewetting phenomenon. It is therefore critical to understand the dewetting mechanisms.

In the past decades, intensive attention has been paid on the film dewetting in the presence of surfactant with a variety of advances made by such as Grotberg and his co-workers and Matar and his co-workers [26-36]. However, due to the highly complex hydrodynamics, along with coupled and susceptive influencing factors, many internal physical mechanisms regarding the surfactant-caused liquid film dewetting have yet to be addressed. For instance, for the dewetting of a water film initiated by surfactant-laden droplet impacting, under what conditions will dewetting happen and what is the dewetting capability of a surfactant-laden droplet? These questions are closely related to the administration of surfactant therapy. In this work, we build an experimental system that allows a surfactant-laden droplet to impact a water film, and investigate the dewetting phenomenon induced by the surfactant-laden droplet by changing the surfactant concentration. We also conduct energy analysis on the dewetting mechanism and establish a linear relation between the maximum dewetting and the surfactant concentration in the film. We expect that these results could not only deepen the understanding on the physics of the film dewetting, but also provide fundamental guidance for surfactant therapy and promote its clinical application.

The surfactant used here is a soluble anionic surfactant Dipotassium dodecyl phosphate (Molecular Formula: $C_{12}H_{25}OPO_3K_2$) with a critical micelle concentration (CMC) of 2.58 mmol/L. Its structure and basic properties can be seen in Supplemental Materials [37]. Aqueous solutions with the surfactant concentration varying from 0.5 to 140 CMC are used to form droplets via an injector equipped with a thin needle. A droplet with a controlled diameter (2.1 or 3.4 mm here) falls from a certain height (5-20 cm) and collides on the surface of the water film. The water film is pancake-shaped with a fixed diameter of 252 mm, and its thickness varies from 0.4 to 1.0 mm in our experiments. See detailed experimental system and conditions in Supplemental Materials [37]. Under the present droplet impacting and water film conditions, the Weber number of the droplet is from 28 to 188 approximately and the ratio of the film thickness to the droplet diameter is from 0.1 to 0.5. Considering the condition of droplet splashing on liquid films established by Cossali et al. [38], no splashing would occur. This has also been verified by the following experimental observations.

When a pure water droplet falls into a water film, impact crater forms first and then capillary waves travel along the crater sidewall until they disappear [39,40]. For the impacting of a surfactant-laden droplet, we observe that the water film exhibits three different behaviors, including non-dewetting, unstable dewetting, and stable dewetting, depending on the surfactant concentration in the droplet (c_{drop}) and the water film thickness (H) (see Video S1-S3 in Supplemental Materials [37]). As shown in Fig. 1(a), if c_{drop} is very small (0.57 CMC) and H is moderate (0.7 mm), almost no obvious difference is detected compared with the pure water droplet impacting, which is noted as “non-dewetting”. When c_{drop} is increased 10 times to 5.7 CMC (H=0.7 mm), dewetting occurs after the impact crater formation, as shown at 54 ms in Fig. 1(b), and the dewetting area expands outwards until reaches a maximum diameter; thereafter, the dewetting area begins to decrease until completely vanishes. This circumstance of the water film is termed as “unstable dewetting”. When further increasing c_{drop}, while reducing H, *i.e.*, c_{drop}=68 CMC and H=0.4 mm, as shown in Fig. 1(c), the dewetting area in the water film spreads further. When it reaches the maximum dewetting diameter, the dewetting area may slightly retract, it does not, however, disappear. This is termed as “stable dewetting”. We find that, in the stable dewetting cases, the maximum dewetting diameter could even reach more than 100 mm, which is 50 times of the droplet diameter (see an example of stable dewetting with 125 mm dewetting diameter in Supplemental Materials [37]).

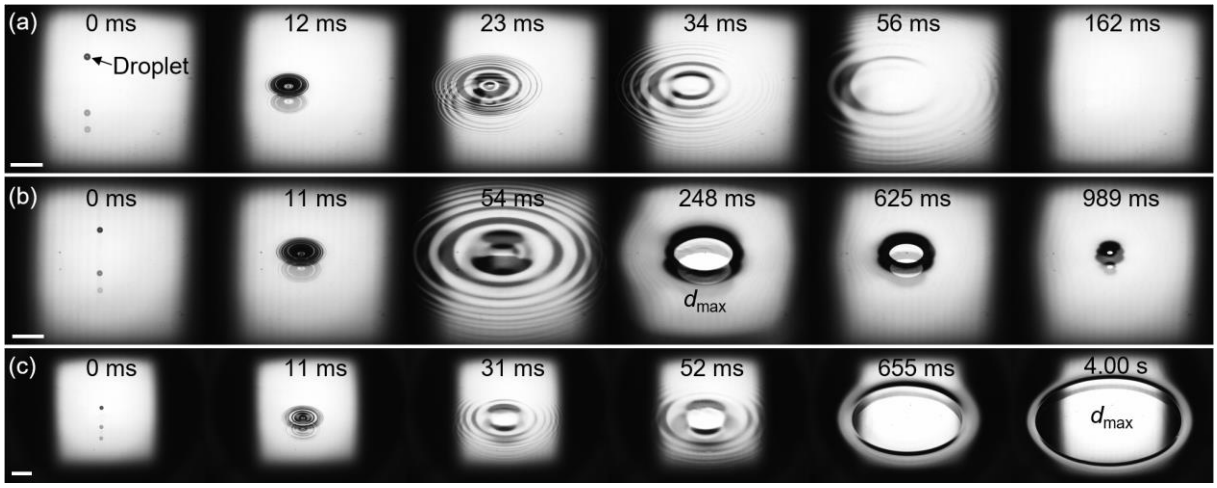

FIG. 1. Three behaviors of water films after surfactant-laden droplets impacting. a) Non-dewetting (c_{drop}=0.57 CMC and H=0.7 mm): impact crater forms after droplet impacting, and then capillary waves propagates outwards until disappear. b) Unstable dewetting (c_{drop}=5.7 CMC and H=0.7 mm): dewetting occurs and expands outwards, but after reaching a maximum dewetting area, rewetting happens and repairs the water film. c) Stable dewetting (c_{drop}=68 CMC and H=0.4 mm): the dewetting area does not disappear and the maximum dewetting diameter is rather large compared to the impacting droplet size. In Fig. 1, all surfactant-laden droplets have diameters of 2.1 mm and impacting heights of 10 cm. The scale bars in Fig. 1 are all 10 mm.

To be more comprehensive, we show a phase diagram in Fig. 2 illustrating three behaviors of the water film after surfactant-laden droplet impacting. The x-axis in the phase diagram is the dimensionless surfactant concentration in the droplet, $c_*=c_{drop}V_{drop}/V_{cap}$ (V_{drop} is the droplet volume, V_{cap} is the volume of a droplet whose diameter is the capillary length, $L_{cap}=(\gamma_{cmc}/\rho g)^{0.5}$, where γ_{cmc} is the surface tension of the aqueous mixture at CMC). The y-axis is a modified Bond number, $Bo=\rho g H^2/\Delta\gamma_{cmc}$, as a function of the water film thickness H and the surface tension difference $\Delta\gamma_{cmc}=\gamma_0-\gamma_{cmc}$ (γ_0 is the surface tension of pure water). From Fig. 2, we conclude that when the conditions move toward the lower right corner of the phase diagram, the water film behavior changes from "non-dewetting" to "stable dewetting", *i.e.*, with larger c_* and smaller Bo, the dewetting effect on the liquid film becomes stronger. Furthermore, the boundaries between different behaviors seem to be straight lines, implying the competition between the Marangoni stress and hydrostatic forces during dewetting. It should be noted that, to trigger dewetting behaviors on a water film via surfactant-laden droplet, the water film should not be too thick. In other words, the Bond number, Bo, should be less than one to ensure the surface tension difference dominates in the process; otherwise, the phase diagram in Fig. 2 is no longer applicable.

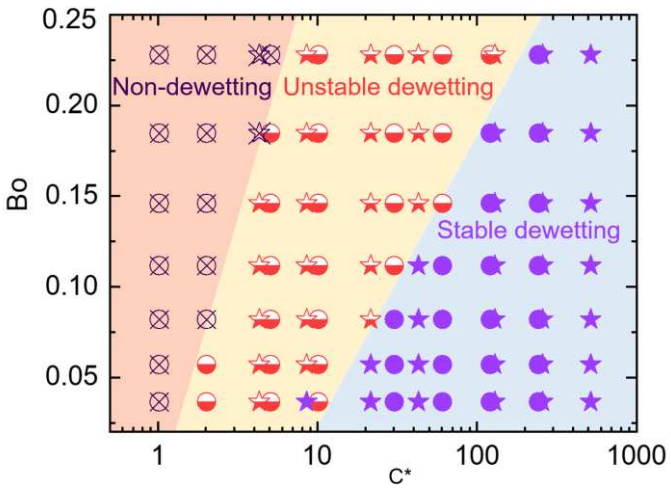

FIG. 2. Phase diagram illustrating three behaviors of water film after surfactant-laden droplet impacting as a function of dimensionless surfactant concentration in the droplet, $c*=c_{drop}V_{drop}/V_{cap}$, and the modified Bond number, $Bo=\rho gH^2/\Delta\gamma_{cmc}$. The phase diagram shows results from two groups of original experiments with one group uses surfactant-laden droplets of 2.1 mm diameter (circular symbols) and the other 3.4 mm diameter (star symbols). Each behavior of the water film is marked by a kind of symbol (crossed symbol, semi-solid symbol, or solid symbol) and the background colors assigned are meant as a guide to the eye.

We attempt to set up a physical model, as described in Fig. 3, to elucidate the water film dewetting phenomenon triggered by surfactant-laden droplet impacting. The droplet penetrates into the liquid film via impacting and then the surfactant molecules in the droplet begin to diffuse due to the concentration gradient, which is governed by the Fick's second law. Simultaneously, the diffused surfactant molecules adsorb onto the liquid-air interface from the bulk liquid, resulting in surface tension gradient, or called the Marangoni stress, to drive the dewetting phenomenon. However, we have to point out that this dewetting is not "perfect" dewetting. There is still a thin film adhering on the solid substrate in the dewetting area. We prove the existence of the thin film and roughly estimate its thickness to be on the order of 10 μm (see Supplemental Materials for details [37]). Experiments by Iasella *et al.* also support our estimation [41]. Thus, in the model illustration Fig. 3(c) and (d), we have drawn a thin water film remains in underneath the dewetting area, but the volume of this residual thin film can be ignored compared to the total liquid volume.

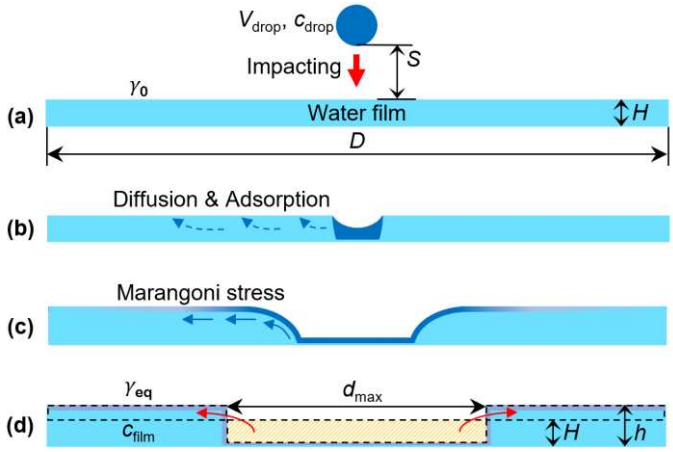

FIG. 3. Schematic of the water film dewetting after impacting of a surfactant-laden droplet. a) Initial state of the droplet and the water film. b) Diffusion and adsorption of surfactant molecules in the water film. c) Marangoni stress drives Marangoni flows inside the water film, causing apparent dewetting phenomenon. d) The state when reaching the maximum dewetting diameter.

We also extract the variations of the square of the dewetting diameter (d^2) with time under different c_{film} before reaching the maximum dewetting. We use c_{film} here to describe the experimental condition for convenience, and c_{film} represents the average surfactant concentrations in the water film after infusing with the surfactant-laden droplet ($c_{film} = c_{drop}V_{drop}/\pi D^2 H$, where D is the water film diameter). As shown in Fig. 4(a) and its subfigure, the curves of d^2 under different c_{film} are all S-type with their slopes first increasing and then decreasing. This kind of changing trend is different from other dewetting characteristics such as evaporation-induced dewetting [42-44]. As mentioned above, the Marangoni stress is the driving force that plays the key role during the dewetting process. Since the surface tension on the liquid-air interface decides the Marangoni stress, we infer that the dynamics of the dewetting closely relates to the dynamic surface tension. According to a series of papers by Hua and Rosen [45-47], the dynamic surface tension curves could be empirically modelled by Eq. (1), which is on a logarithmic time-scale, regardless of surfactant concentration or type.

$$\Delta\gamma = \Delta\gamma_{max} - \frac{\Delta\gamma_{max}}{1+(t/t_0)^p} \quad (1)$$

where $\Delta\gamma$ is γ_0–γ which means the real-time surface tension reduction after addition of surfactant, and $\Delta\gamma_{max}$ is γ_0–γ_{eq} meaning the final surface tension reduction at c_{film} (γ_{eq} is the equilibrium surface tension); t_0 is a constant with time dimension, and p is a dimensionless constant. Coincidentally, when we change the x-axis from t to $\Delta\gamma$, and replot the variations of d^2, we see that the original curves, which are scattered in Fig. 4(a), all collapse onto a single line in Fig. 4(b). This result proves our inference that the dynamic surface tension reduction correlates the dewetting dynamics.

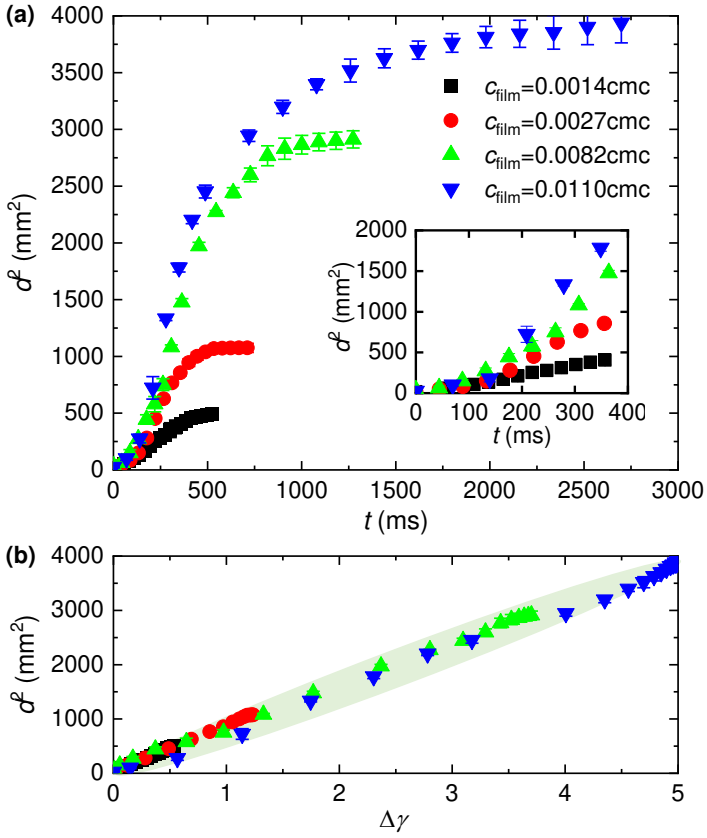

FIG. 4. Variations of the square of dewetting diameter (d^2). a) Time-varied d^2 under different surfactant concentrations in the water film (c_{film}) before reaching the maximum dewetting. The subfigure shows data at earlier times more clearly. b) Replotting the variations of d^2 with the dynamic surface tension reduction, $\Delta\gamma$. Curves under different c_{film} collapse onto one single line (the background color assigned is meant as a guide to the eye). Error bars in the figure display the standard deviations of parallel measurements.

Mechanically, the dewetting phenomenon is governed by the Marangoni stress, the viscous force and the gravity. The dewetting takes place when the Marangoni stress overcome the latter two forces. From another view of energy conversion, the essence of the dewetting could be described as that the reduced surface energy due to the addition of surfactant is converted into the gravitational energy of partial water film (those water in the shadow box in Fig. 3(d)) after overcoming the viscous dissipation. It should be noted that the sum of the kinetic energy and the surface energy of the impacting droplet is calculated to be at least two orders of magnitude smaller than the surface energy of the water film and then can be neglected. Based on this viewpoint, an energy conversion model is established more straightforwardly, which is described by $\Delta E_{sur} = G + E_{vis}$ or $k\Delta E_{sur} = G$, where ΔE_{sur} is the reduced surface energy of the water film due to the addition of surfactant, G is the increased gravitational energy of partial water film, E_{vis} is the viscous dissipation, and k represents the energy conversion rate from ΔE_{sur} to G. Considering the "imperfect" dewetting that there is still thin fluid layer in the dewetting area, when the maximum dewetting is reached (Fig. 3(d)), the surface energy reduction of the water film, ΔE_{sur}, can be calculated as

$$\Delta E_{sur} = \frac{\pi D^2(\gamma_0 - \gamma_{eq})}{4} \propto D^2 \Delta\gamma_{max} \quad (2)$$

The increased gravitational potential energy, G, caused by the rise of the water level is given by

$$G = \frac{\pi\rho g D^2 H^2 d_{max}^2}{8(D^2 - d_{max}^2)} \propto \frac{D^2 H^2 d_{max}^2}{D^2 - d_{max}^2} \tag{3}$$

Base on the energy conversion principle, $k\Delta E_{sur} = G$, we have

$$k\Delta\gamma_{max} \propto \frac{H^2 d_{max}^2}{D^2 - d_{max}^2} \tag{4}$$

The energy conversion rate k can be obtained from experiments, and we are pleasantly surprised to find that k is proportional to the square of H, regardless of other experimental conditions, as shown in Fig. 5(a). Therefore, Equation (4) becomes $\Delta\gamma_{max} \propto d_{max}^2/(D^2 - d_{max}^2)$. In our experiments, D^2 is at least an order of magnitude larger than d_{max}^2, and considering the constant D, we get $d_{max}^2 \propto \Delta\gamma_{max}$. Actually, in Fig. 4(b), if let t to be infinitely large to reach d_{max}, we can also get the same conclusion, $d_{max}^2 \propto \Delta\gamma_{max}$.

Combining Gibbs isotherm and Langmuir isotherm yields

$$\Delta\gamma_{max} = NRT\Gamma \ln(1 + bc_{film}) \tag{5}$$

where Γ is the saturated surface excess of a surfactant, T is Kelvin temperature, R is gas molecular constant, and N and b are constants. If the surfactant type and the temperature are determined, all these parameters keep unchanged. Under the conditions that the surfactant concentration is very low (*e.g.*, in our experiments c_{film} is normally less than 0.01 CMC), Equation (5) could be simplified as $\Delta\gamma_{max} \propto c_{film}$. Thus, we obtain

$$d_{max}^2 \propto c_{film} \tag{6}$$

The data points in Fig. 5(b) validate Eq. (6) very well. However, deviations from the scaling of Eq. (6) appear for c_{film} exceeding 0.01 CMC, which are mainly attributed to two reasons. First, Equation (4) cannot be simplified, as d_{max}^2 is not small anymore compared to D^2. Second, the simplification of Eq. (5) is not appropriate for relatively large c_{film}. In addition, as shown in Fig. 5(b), within our experimental conditions, the impacting height of the surfactant-laden droplet, S, does not have obvious influence on the result, because such impacting heights cannot cause droplet splashing on water films [38]. We infer that with serious droplet splashing, the maximum dewetting does not satisfy the scaling of Eq. (6) anymore, which needs further investigation.

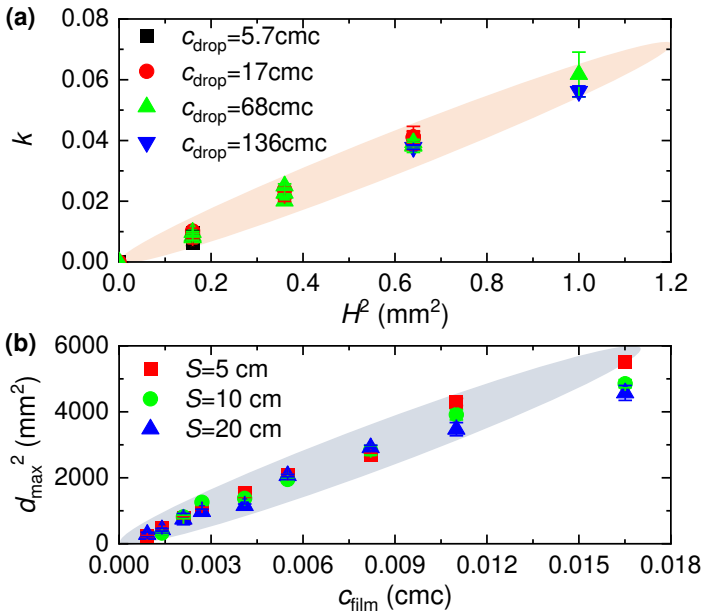

FIG. 5. a) Experimentally obtained proportional relation between the energy conversion rate (k) and the square of water film thickness (H^2). b) Theoretically deduced proportional relation between the square of the maximum dewetting diameter (d_{max}^2) and c_{film}, and its validation. The background color assigned are guides to the eye. Error bars in the figure display the standard deviations of parallel measurements.

In summary, we investigate the water film dewetting initiated by surfactant-laden droplet impacting, determine the dewetting capability of the surfactant-laden droplet, and elucidate the underlying physical mechanisms. Three behaviors of the water film after a surfactant-laden droplet impacting are characterized, including non-dewetting, unstable dewetting, and stable dewetting, with a phase diagram drawn to distinguish them. For the dewetting behaviors, S-type variations of the dewetting area are identified, which is demonstrated to be closely related to the dynamic surface tension reduction. A linear relation between the maximum dewetting and the surfactant concentration in the film is also established based on the energy conversion from surface energy to gravitational energy, and the energy conversion rate linearly relates to the square of the water film thickness. We expect that these results pioneer in understanding the principle of water film dewetting initiated by surfactant, which could further guide practical applications such as the pulmonary surfactant therapy.

This work was supported by the National Natural Science Foundation of China (No. 51876007), the Fundamental Research Funds for the Central Universities (No. FRF-BD-20-09A), and the Integrated Projects utilizing the Space Environment on ISS and CSS supported by CMSA and ESA (No. TGMTYY00-RW-03). The authors also acknowledge fruitful discussions with Dr. Yaxing Li from Physics of Fluids group, University of Twente.

References

[1] COVID-19 Dashboard by the Center for Systems Science and Engineering at Johns Hopkins University (JHU), https://coronavirus.jhu.edu/map.html.

[2] C. G. K. Ziegler et al., SARS-CoV-2 Receptor ACE2 Is an Interferon-Stimulated Gene in Human Airway Epithelial Cells and Is Detected in Specific Cell Subsets across Tissues, Cell 181, 1016 (2020).

[3] A. M. Arvin, K. Fink, M. A. Schmid, A. Cathcart, R. Spreafico, C. Havenar-Daughton, A. Lanzavecchia, D. Corti, and H. W. Virgin, A perspective on potential antibody-dependent enhancement of SARS-CoV-2, Nature 584, 353 (2020).

[4] D. Wrapp, N. S. Wang, K. S. Corbett, J. A. Goldsmith, C. L. Hsieh, O. Abiona, B. S. Graham, and J. S. McLellan, Cryo-EM structure of the 2019-nCoV spike in the prefusion conformation, Science 367, 1260 (2020).

[5] M. Feldmann, R. N. Maini, J. N. Woody, S. T. Holgate, G. Winter, M. Rowland, D. Richards, and T. Hussell, Trials of anti-tumour necrosis factor therapy for COVID-19 are urgently needed, Lancet 395, 1407 (2020).

[6] J. A. Clements, Surfactant in pulmonary disease, N. Engl. J. Med. 272, 1336 (1965).

[7] E. J. Veldhuizen and H. P. Haagsman, Role of pulmonary surfactant components in surface film formation and dynamics, Biochim. Biophys. Acta 1467, 255 (2000).

[8] J. S. Ayres, A metabolic handbook for the COVID-19 pandemic, Nat. Metab. 2, 572 (2020).

[9] M. Abkarian and H.A. Stone, Stretching and break-up of saliva filaments during speech: A route for pathogen aerosolization and its potential mitigation Phys. Rev. Fluids 5, 102301(R) (2020).

[10] F. Yang, A.A. Pahlavan, S. Mendez, M. Abkarian, and H.A. Stone, Towards improved social distancing guidelines: Space and time dependence of virus transmission from speech-driven aerosol transport between two individuals, Phys. Rev. Fluids, 5, 122501(R) (2020).

[11] K. L. Chong, C. S. Ng, N. Hori, R. Yang, R. Verzicco, and D. Lohse, Extended Lifetime of Respiratory Droplets in a Turbulent Vapor Puff and Its Implications on Airborne Disease Transmission, Phys. Rev. Lett. 126, 034502 (2021).

[12] H. Zhong, Z. Zhu, P. You, J. Lin, C. F. Cheung, V. L. Lu, F. Yan, C. Y. Chan, and G. Li, Plasmonic and Superhydrophobic Self-Decontaminating N95 Respirators, ACS Nano 14, 8846 (2020).

[13] C. D. Zangmeister, J. G. Radney, E. P. Vicenzi, and J. L. Weaver, Filtration Efficiencies of Nanoscale Aerosol by Cloth Mask Materials Used to Slow the Spread of SARS-CoV-2, ACS Nano 14, 9188 (2020).

[14] F. J. Garcia de Abajo, R. J. Hernandez, I. Kaminer, A. Meyerhans, J. Rosell-Llompart, and T. Sanchez-Elsner, Back to Normal: An Old Physics Route to Reduce SARS-CoV-2 Transmission in Indoor Spaces, ACS Nano 14, 7704

(2020).
[15] M. Raeiszadeh and B. Adeli, A Critical Review on Ultraviolet Disinfection Systems against COVID-19 Outbreak: Applicability, Validation, and Safety Considerations, ACS Photonics 7, 2941 (2020).
[16] Y. Y. Zuo, W. E. Uspal, and T. Wei, Airborne Transmission of COVID-19: Aerosol Dispersion, Lung Deposition, ACS Nano 14, 16502 (2020).
[17] A. Z. Stetten, S. V. Iasella, T. E. Corcoran, S. Garoff, T. M. Przybycien, and R. D. Tilton, Surfactant-induced Marangoni transport of lipids and therapeutics within the lung, Curr. Opin. Colloid Interface Sci. 36, 58 (2018).
[18] R. Weiskirchen, Severity of Coronavirus Disease 2019 (COVID-19): Does Surfactant Matter? Front. Microbiol. 11, 1905 (2020).
[19] M. L. Smith, S. Gandolfi, P. M. Coshall, and P. Rahman, Biosurfactants: A Covid-19 Perspective, Front. Microbiol. 11, 1341 (2020).
[20] S. Piva et al., Surfactant therapy for COVID-19 related ARDS: a retrospective case–control pilot study, Respir. Res. 22, 20 (2021).
[21] T. Fujiwara, S. Chida, Y. Watabe, H. Maeta, T. Morita, and T. Abe, Artificial surfactant therapy in hyaline-membrane disease, Lancet 315, 55 (1980).
[22] A. H. Jobe, Pulmonary surfactant therapy, N. Engl. J. Med. 328, 861 (1993).
[23] R. Hentschel, K. Bohlin, A. van Kaam, H. Fuchs, and O. Danhaive, Surfactant replacement therapy: from biological basis to current clinical practice, Pediatr. Res. 88, 176 (2020).
[24] T. P. Stevens and R. A. Sinkin, Surfactant replacement therapy, Chest 131, 1577 (2007).
[25] P. J. Papadakos and B. Lachmann, Mechanical ventilation: clinical applications and pathophysiology (Saunders Elsevier, Philadelphia, 2008).
[26] A. B. Afsar-Siddiqui, P. F. Luckham, and O. K. Matar, The spreading of surfactant solutions on thin liquid films, Adv. Colloid Interface Sci. 106, 183 (2003).
[27] R. V. Craster and O. K. Matar, Dynamics and stability of thin liquid films, Rev. Mod. Phys. 81, 1131 (2009).
[28] D. Langevin, On the rupture of thin films made from aqueous surfactant solutions, Adv. Colloid Interface Sci. 275, 102075 (2020).
[29] D. Halpern and J. B. Grotberg, Dynamics and transport of a localized soluble surfactant on a thin film, J. Fluid Mech. 237, 1 (1992).
[30] O. E. Jensen and J. B. Grotberg, Insoluble surfactant spreading on a thin viscous film: shock evolution and film rupture, J. Fluid Mech. 240, 259 (1992).
[31] A. B. Afsar-Siddiqui, P. F. Luckham, and O. K. Matar, Unstable Spreading of Aqueous Anionic Surfactant Solutions on Liquid Films. 2. Highly Soluble Surfactant, Langmuir 19, 703 (2003).
[32] A. B. Afsar-Siddiqui, P. F. Luckham, and O. K. Matar, Dewetting behavior of aqueous cationic surfactant solutions on liquid films, Langmuir 20, 7575 (2004).
[33] K. S. Lee and V. M. Starov, Spreading of surfactant solutions over thin aqueous layers at low concentrations: Influence of solubility, J. Colloid Interface Sci. 329, 361 (2009).
[34] M. Roché, Z. Li, I. M. Griffiths, S. Le Roux, I. Cantat, A. Saint-Jalmes, and H. A. Stone, Marangoni Flow of Soluble Amphiphiles, Phys. Rev. Lett. 112, 208302 (2014).
[35] J. V. Goddard and S. Naire, The spreading and stability of a surfactant-laden drop on an inclined prewetted substrate, J. Fluid Mech. 772, 535 (2015).
[36] Z. Che and O. K. Matar, Impact of Droplets on Liquid Films in the Presence of Surfactant, Langmuir 33, 12140 (2017).
[37] See Supplemental Materials at [URL] for supplemental contents and videos S1–S3.
[38] G. E. Cossali, A. Coghe, and M. Marengo, The impact of a single drop on a wetted solid surface, Exp. Fluids 22, 463 (1997).
[39] C. Josserand, P. Ray, and S. Zaleski, Droplet impact on a thin liquid film: anatomy of the splash, J. Fluid Mech. 802,

775 (2016).

[40] E. Berberovic, N. P. van Hinsberg, S. Jakirlic, I. V. Roisman, and C. Tropea, Drop impact onto a liquid layer of finite thickness: dynamics of the cavity evolution, Phys. Rev. E 79, 036306 (2009).

[41] S. V. Iasella, N. Sun, X. Zhang, T. E. Corcoran, S. Garoff, T. M. Przybycien, and R. D. Tilton, Flow regime transitions and effects on solute transport in surfactant-driven Marangoni flows, J. Colloid Interface Sci. 553, 136 (2019).

[42] P. K. Roy, M. Frenkel, I. Legchenkova, S. Shoval, B. P. Binks, and E. Bormashenko, Liquid Marble-Induced Dewetting, J. Phys. Chem. C 124, 9345 (2020).

[43] S. Kim, J. Kim, and H.-Y. Kim, Dewetting of liquid film via vapour-mediated Marangoni effect, J. Fluid Mech. 872, 100 (2019).

[44] S. Kim, J. Kim, and H.-Y. Kim, Formation, growth, and saturation of dry holes in thick liquid films under vapor-mediated Marangoni effect, Phys. Fluids 31, 112105 (2019).

[45] X. Y. Hua and M. J. Rosen, Dynamic Surface Tension of Aqueous Surfactant Solutions, J. Colloid Interface Sci. 124, 652 (1988).

[46] M. J. Rosen and X. Y. Hua, Dynamic surface tension of aqueous surfactant solutions: 2. Parameters at 1 s and at mesoequilibrium, J. Colloid Interface Sci. 139, 397 (1990).

[47] X. Y. Hua and M. J. Rosen, Dynamic surface tension of aqueous surfactant solutions: 3. Some effects of molecular structure and environment, J. Colloid Interface Sci. 141, 180 (1991).